Journal of Hepatocellular Carcinoma

Dovepress
Taylor & Francis Group

Open Access Full Text Article

ORIGINAL RESEARCH

Predictive Value of IDEAL-IQ and DWI Imaging Biomarkers for P53 Mutations in Hepatocellular Carcinoma

Dongdong Wang[1,*], Huijia Yin[2,*], Xiaoming Li[1], Shuwei Zhou[3], Yuan-Cheng Wang[3]

[1]Department of Radiology, Zhengzhou People's Hospital and The Fifth Clinical Medical College of Henan University of Chinese Medicine, Zhengzhou, People's Republic of China; [2]Department of MR, The First Affiliated Hospital of Xinxiang Medical University, Weihui, People's Republic of China; [3]Department of Radiology, Zhongda Hospital, Nurturing Center of Jiangsu Province for State Laboratory of AI Imaging and Interventional Radiology, School of Medicine, Southeast University, Nanjing, People's Republic of China

*These authors contributed equally to this work

Correspondence: Yuan-Cheng Wang, Department of Radiology, Zhongda Hospital, Nurturing Center of Jiangsu Province for State Laboratory of AI Imaging and Interventional Radiology, School of Medicine, Southeast University, Nanjing, 210009, People's Republic of China, Tel +86 25 83272121, Fax +86 25 83311083, Email yuancheng_wang@seu.edu.cn

Purpose: To investigate the application of imaging biomarkers, including R2*, Fat Fraction (FF) and apparent diffusion coefficient (ADC) values, obtained through Iterative Decomposition of water and fat with Echo Asymmetry and Least-squares estimation for Imaging Quantification (IDEAL-IQ) and DWI techniques, in differentiating P53-mutated and non-mutated HCC.

Patients and Methods: This retrospective study included patients with pathologically confirmed HCC between January 2019 and July 2024. HCC were divided into P53-mutated group and non-mutated group by immunostaining. Preoperative R2*, FF, and ADC values derived from IDEAL-IQ and DWI were compared between the two groups, as well as different histological grades. Receiver operating characteristic (ROC) analysis was used to evaluate the diagnostic performance of each MRI parameter for detecting P53 mutations in HCC, with area under the curve (AUC) compared by Delong's test.

Results: Compared to the non-mutated group, the P53-mutated group (n = 31) showed significantly higher R2* values (34.821 ± 9.980 vs 23.713 ± 5.586, P < 0.001) and lower ADC values (0.760 ± 0.142 vs 0.855 ± 0.130, P = 0.002), while FF values showed no significant difference (P = 0.646). R2*, ADC, and the combined model (R2* + ADC) revealed AUCs of 0.849, 0.726, and 0.856, respectively, with the combined model demonstrating the highest sensitivity and specificity. Additionally, high-grade HCC showed significantly lower ADC values compared to lower-grade tumors (P < 0.001).

Conclusion: R2* and ADC exhibited significant features in P53-mutated HCC, suggesting their potential as non-invasive biomarkers for predicting P53 mutation status and guiding clinical management. The combined use of R2* and ADC may further enhance diagnostic accuracy.

Keywords: hepatocellular carcinoma, P53-mutated, magnetic resonance imaging, diffusion weighted imaging, iterative decomposition of water and fat with echo asymmetry and least squares estimation

Introduction

Hepatocellular carcinoma (HCC) is the most common primary liver cancer, with high morbidity and mortality rates,[1] making it a global health issue. Despite continuous efforts to explore and try various treatments to extend patient survival, the incidence of postoperative metastasis and recurrence remains high in recent years, leading to limited improvement in patient prognosis.[2]

HCC is characterized by pronounced spatial heterogeneity due to genomic instability and microenvironmental interactions.[3,4] This heterogeneity contributes to variable treatment responses and complicates prognosis prediction,[4] underscoring the need for biomarkers enabling personalized therapeutic strategies. Identifying biomarkers associated with poor prognosis is of significant clinical importance for the early diagnosis and targeted treatment of HCC. The P53

Received: 18 March 2025
Accepted: 26 July 2025
Published: 6 August 2025

protein is encoded by the TP53 gene located on human chromosome 17.[5] P53 was originally identified as a tumor suppressor gene and plays an essential role in inhibiting cancer development. It is activated when cells undergo stress, thus preventing uncontrolled cell division and proliferation.[6] P53 mutations are common genetic abnormalities that are typically not expressed in the healthy adult liver.[7] In HCC, P53 mutations are closely associated with tumor generation and progression, as well as with the invasiveness and prognosis,[8,9] and the P53 gene has become a promising drug target in cancer therapy.[10] Molecular classification studies reveal distinct HCC subtypes: P53 mutations cluster predominantly in the proliferation class, the major molecular subtype of HCC defined by dysregulated cell-cycle pathways, including progenitor-like subtypes (characterized by stemness traits such as EPCAM and CK19 expression) and Wnt-TGFβ-activated subtypes (defined by dysregulated Wnt/β-catenin signaling). Conversely, TP53-wild-type tumors predominantly fall into the non-proliferation class with preserved DNA repair and angiogenesis-dominant phenotypes.[11] This molecular heterogeneity necessitates non-invasive stratification tools. Clinical studies confirm that TP53 hotspot mutations (R249S/V157F) are associated with poor prognosis in HCC. The acquisition of stem cell-like gene expression traits may contribute to the aggressive behavior of P53-mutated tumors.[12] Consequently, early identification of P53-mutated HCC has great clinical value for treatment selection and prognosis assessment.

Currently, liver biopsy is considered the reference standard for preoperative diagnosis of P53 mutation expression; however, it cannot reflect the heterogeneity of the entire tumor and, as an invasive procedure, carries certain risks and limitations. Therefore, non-invasive imaging methods have been a research focus. Thus, it is essential to develop a valuable non-invasive imaging method to evaluate and predict the P53 mutation status of HCC before liver resection.

Diffusion Weighted Imaging (DWI) is a basic imaging technique that reflects the microstructure and physiological state of tissues at the molecular level by measuring the diffusion of water molecules within tissues. In HCC, DWI can non-invasively assess the cellular density and microenvironmental changes in tumor tissue, which is crucial for tumor detection, grading, and treatment evaluation.[13,14] Iterative Decomposition of water and fat with Echo Asymmetry and Least-squares estimation for Imaging Quantification (IDEAL-IQ) is a quantitative magnetic resonance imaging sequence that reflects tissue microstructure, enabling effective analysis of water and fat content and precise measurement of Fat Fraction (FF) in tissue (reflected by FF) and iron deposition (reflected by R2*).[15] IDEAL-IQ has been widely used in the evaluation of lesions in the central nervous system, musculoskeletal system, liver, and rectum.[16–19] However, to date, there have been no studies using IDEAL-IQ technology to predict P53 mutations in HCC.

Therefore, this study explores the application of imaging biomarkers obtained through IDEAL-IQ and DWI technologies (such as R2*, FF, and ADC values) in distinguishing P53-mutated from non-mutated HCC, providing new insights for the diagnosis and treatment of HCC.

Materials and Methods

Patients

This retrospective study was approved by the Ethics Committee of Zhengzhou People's Hospital (Approval number: 2023011103). The requirement for written informed consent was waived by the Ethics Committee due to the retrospective analysis of anonymized patient data. All data were handled with strict confidentiality measures and complied with the principles of the Declaration of Helsinki. Between January 2019 and July 2024, 299 patients with suspected HCC were selected for liver MRI, including IDEAL-IQ, DWI, and conventional MRI sequences. The inclusion criteria were as follows: (1) HCC confirmed by surgical pathology; (2) pathological confirmation of P53 expression (positive or negative) by immunohistochemistry and availability of Edmondson-Steiner grading data; (3) acceptable preoperative image quality for IDEAL-IQ and DWI sequences; and (4) the interval between obtaining the pathological specimen and MRI scanning did not exceed two weeks. Exclusion criteria were: (1) lesions too small to delineate a region of interest (ROI); and (2) a history of any other treatments for HCC. Finally, 65 patients were included in this study (Figure 1).

Histopathological Analysis

A liver pathologist with 15 years of experience reviewed all HCC specimens. Immunohistochemistry was used to divide HCC patients into P53-mutated and non-P53-mutated groups based on the proportion of P53-positive cells. The

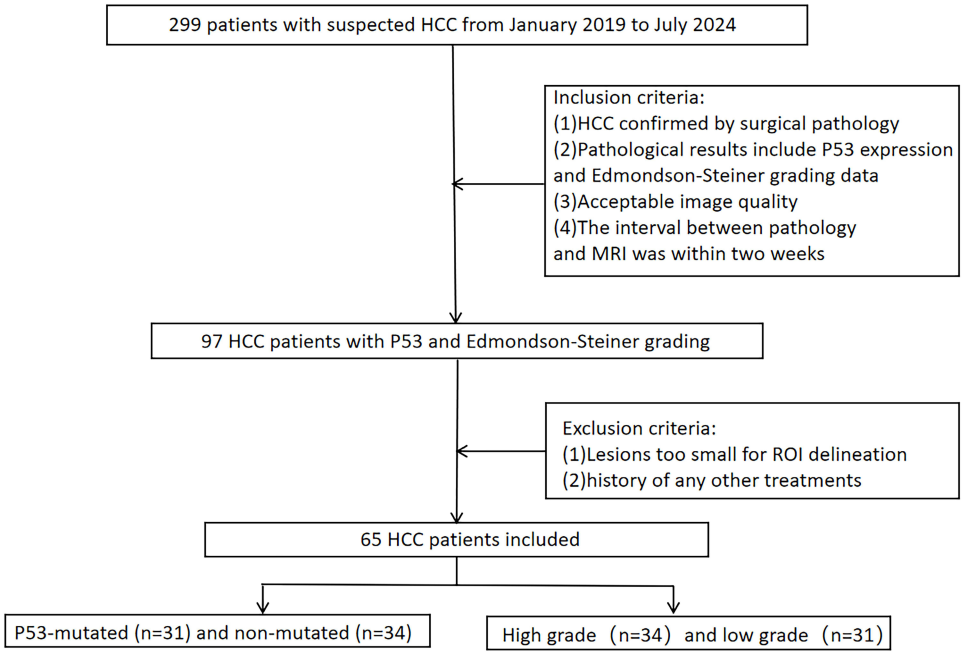

Figure 1 Flow diagram for the inclusion and exclusion criteria.

expression of P53 in tumor tissue was scored according to the percentage of cells with positive nuclear staining, with P53 mutation defined as a proportion of ≥10%.[9,20]

MR Scanning Protocols

All patients were examined with a 3.0 T MR scanner (Discovery MR750, GE Healthcare, Waukesha, WI, USA) with a 32-channel phased-array body coil. The protocol was as follows: an axial T2-weighted fast spin-echo (FSE) sequence with repetition time (TR) 4285 ms, echo time (TE) 73.1 ms, flip angle 120°, FOV 400×400 mm^2, bandwidth 325 Hz, and slice thickness 5 mm; an axial breath-hold T1-weighted 3D fat suppressed spoiled gradient-echo sequence with liver acquisition and volume acceleration and TR 4.1 ms, TE 1.9 ms, flip angle 12°, FOV 400×400 mm^2; DWI with transverse single-shot spin-echo echo-planar sequences (b values, 0 and 800s/mm^2); an axial breath-hold IDEAL-IQ sequence with TR 6.1 ms, effective TE 2.8 ms, flip angle 3°, field of view (FOV) 400×400 mm^2, bandwidth 1302 Hz, and slice thickness 5 mm.

Image Processing and Analysis

All image assessments were performed on a post-processing workstation (AW 4.6, GE Healthcare, USA). Two experienced abdominal radiologists (with 6 and 15 years of MRI diagnostic experience, respectively) independently reviewed the images and were blinded to clinical and pathological information. The R2*, FF, and ADC values of HCC were measured on corresponding original images. Regions of interest (ROIs) were manually delineated on the largest slice of the lesion, referring to T2WI and contrast-enhanced MR images to confirm the lesion. ROIs were drawn at different locations within the solid portion of the tumor, carefully avoiding cystic or necrotic areas. To minimize measurement errors, consistent ROIs were maintained for each patient. Each radiologist measured the lesions three times, and the average of these three measurements was calculated. The final result was obtained by averaging the measurements from the two radiologists. In patients with multiple tumors, the largest tumor is assessed for evaluation.

Statistical Analysis

The consistency of R2*, FF, and ADC values between the two radiologists was evaluated using the intraclass correlation coefficient (ICC) and its 95% confidence interval (CI): slight agreement (0–0.20), fair agreement (0.21–0.40), moderate

 https://doi.org/10.2147/JHC.S524533

agreement (0.41–0.60), substantial agreement (0.61–0.80), and perfect agreement (0.81–1).[21] The Kolmogorov–Smirnov test was used to assess whether the quantitative parameters followed a normal distribution. Data with a normal distribution were expressed as mean ± standard deviation, while non-normally distributed data were expressed as median (25th, 75th percentiles). Independent sample *t*-tests or Mann–Whitney *U*-tests were used to evaluate differences in parameters between different P53 expression statuses and Edmondson-Steiner grades. Fisher's exact test was applied to detect the correlation between P53 expression status and Edmondson-Steiner grade. Receiver operating characteristic (ROC) curves were used to evaluate the predictive performance of MRI parameters for different P53 expression statuses in HCC. The DeLong's test was used to compare the differences in the area under the curve (AUC) among the parameters and the combined model. Statistical analyses were performed using SPSS software version 26.0 (IBM SPSS Statistics, Armonk, NY) and MedCalc software version 22.0 (MedCalc, Mariakerke, Belgium). $P < 0.05$ was considered statistically significant.

Results

Clinical Characteristics

Among the 65 patients, 31 were in the P53-mutated group and 34 in the non-P53-mutated group. High-grade tumors (Edmondson-Steiner grade III: 30 cases, grade IV: 4 cases) were observed in 34 patients, while low-grade tumors (Edmondson-Steiner grade I: 11 cases, grade II: 20 cases) were found in 31 patients. The mean age of the P53-mutated group was 54.54 ± 9.58 years, compared to 59.03 ± 9.39 years in the non-P53-mutated group. The median AFP level of P53-mutated group was significantly higher than that of non-P53-mutated group (113.100 vs 7.040, respectively) ($P < 0.05$). There were no significant differences between the two groups in terms of sex, tumor count, and tumor size ($P > 0.05$). Similarly, no significant differences were observed in AST and ALT levels between the two groups ($P > 0.05$) (Table 1).

Interobserver Agreement

The Kolmogorov–Smirnov test showed that R2* ($P = 0.200$) and ADC ($P = 0.098$) values followed a normal distribution, while FF ($P < 0.05$) did not. The intraclass correlation coefficient (ICC) demonstrated excellent interobserver agreement for the quantitative measurements of R2*, FF, and ADC values, with ICC values of 0.959 (95% CI: 0.933–0.975), 0.976 (95% CI: 0.961–0.985), and 0.962 (95% CI: 0.939–0.977), respectively.

Table 1 Baseline Characteristics

Parameters	P53-Mutated (n=31)	Non-P53-Mutated (n=34)	P value
Age (years)[a]	54.54 ± 9.58	59.03 ± 9.39	0.060
Sex			0.145
Male	23 (74.19%)	30 (88.24%)	
Female	8 (25.81%)	4 (11.76%)	
Edmondson-Steiner grade			0.060
Low grade (I, II)	11 (35.48%)	20 (58.82%)	
High grade (III, IV)	20 (64.52%)	14 (41.18%)	
AFP (ng/mL)	113.10 (16.65, 428.00)	7.04 (3.24, 33.34)	0.001
No. of tumors			0.727
Solitary	25 (80.65%)	30 (80.24%)	
2–3 tumors	5 (16.13%)	3 (8.82%)	
>3 tumors	1 (3.22%)	1 (2.94%)	
Tumor size (cm)	3.87 (2.39, 5.73)	3.69 (2.37, 5.51)	0.674
AST (IU/L)	43.30 (26.10, 56.30)	27.95 (23.18, 39.85)	0.062
ALT (IU/L)	40.70 (25.70, 63.30)	35.30 (26.30, 47.13)	0.245

Notes: Data are medians with interquartile range in parentheses, or numbers of patients with percentage in parentheses. [a]Data are means ± standard deviations.
Abbreviations: AST, Aspartate aminotransferase; ALT, Alanine Aminotransferase.

Comparisons of DWI and IDEAL-IQ-Derived Parameters

We conducted statistical analysis on different P53 expression statuses in HCC patients. The results showed that the R2* value in the P53-mutated group was significantly higher than in the non-P53-mutated group (34.821 ± 9.980 vs 23.713 ± 5.586, P < 0.001). Additionally, the ADC value in the P53-mutated group was significantly lower than in the non-P53-mutated group (0.760 ± 0.142 vs 0.855 ± 0.130, P = 0.002). However, there was no statistically significant difference in the median FF values between the P53-mutated and non-P53-mutated groups (3.501% vs 3.645%, P = 0.646). Furthermore, we compared the R2*FF, and ADC values between low-grade and high-grade HCC. The results indicated that the ADC value in low-grade HCC was higher than in high-grade HCC (0.877 ± 0.132 vs 0.743 ± 0.127, P < 0.001) (Tables 2, 3 and Figures 2–4).

ROC Curve Analysis

Table 4 shows the diagnostic performance of R2*, ADC, and the combined model (R2* + ADC) for different P53 expression statuses. The AUC values for R2*, ADC, and the combined model (R2* + ADC) were 0.849 (95% CI: 0.739–0.926), 0.726 (95% CI: 0.602–0.830), and 0.856 (95% CI: 0.747–0.931), respectively. The DeLong's test showed a statistically significant difference in AUC between ADC and the combined model (P = 0.039), while there was no statistically significant difference between R2* and the combined model (P = 0.741) (Figure 5 and Table 4).

The Relationship Between Edmonson-Steiner Grade and P53-Mutated

P53 mutation showed a significant association with Edmonson grade (P = 0.032). Figure 6 presents a bar chart of the distribution of Edmonson-Steiner grades in the P53-mutated and non-mutated groups, allowing a clear view of the distribution of P53-mutated and non-mutated samples across different grades. In the Edmonson-Steiner grade III (poorly differentiated) group, the number of samples was highest, regardless of P53 mutation status. The number of samples in the Edmonson-Steiner grade I (well-differentiated) and grade IV (undifferentiated) groups were relatively fewer. From the figure, we can conclude that P53-mutated samples are more concentrated in higher-grade (Edmonson III and IV) HCC patients, suggesting that P53 mutation may be associated with poorer differentiation. In contrast, non-mutated samples are mainly distributed in the moderately differentiated (Edmonson grade II) group, indicating that the incidence of P53 mutations may be lower in highly differentiated tumors.

Table 2 IDEAL-IQ and DWI Parameters of HCC with Different P53 Expression Status

Parameters	P53-Mutated (n=31)	Non-P53-Mutated (n=34)	t/z	P value
R2* (sec^{-1})[a]	34.821 ± 9.980	23.713 ± 5.586	5.601	< 0.001
FF (%)	3.501 (3.273, 4.941)	3.645 (3.197, 5.328)	−0.46	0.646
ADC ($\times 10^{-3}$ mm^2/s)[a]	0.760 ± 0.142	0.855 ± 0.130	−3.196	0.002

Notes: Data are medians with interquartile range in parentheses, unless otherwise specified. [a]Data are means ± standard deviations.
Abbreviations: FF, Fat fraction; ADC, Apparent diffusion coefficient.

Table 3 IDEAL-IQ and DWI Parameters of HCC with Different Histological Grades

Parameters	High Grade (n=34)	Low Grade (n=31)	t/z	P value
R2* (sec^{-1})[a]	30.928 ± 9.609	26.909	1.693	0.095
FF (%)	3.308 (2.633, 4.946)	3.611 (2.742, 5.274)	−0.066	0.948
ADC ($\times 10^{-3}$ mm^2/s)[a]	0.743 ± 0.127	0.877 ± 0.132	−4.16	<0.001

Notes: Data are medians with interquartile range in parentheses, unless otherwise specified. [a]Data are means ± standard deviations.
Abbreviations: FF, Fat fraction; ADC, Apparent diffusion coefficient.

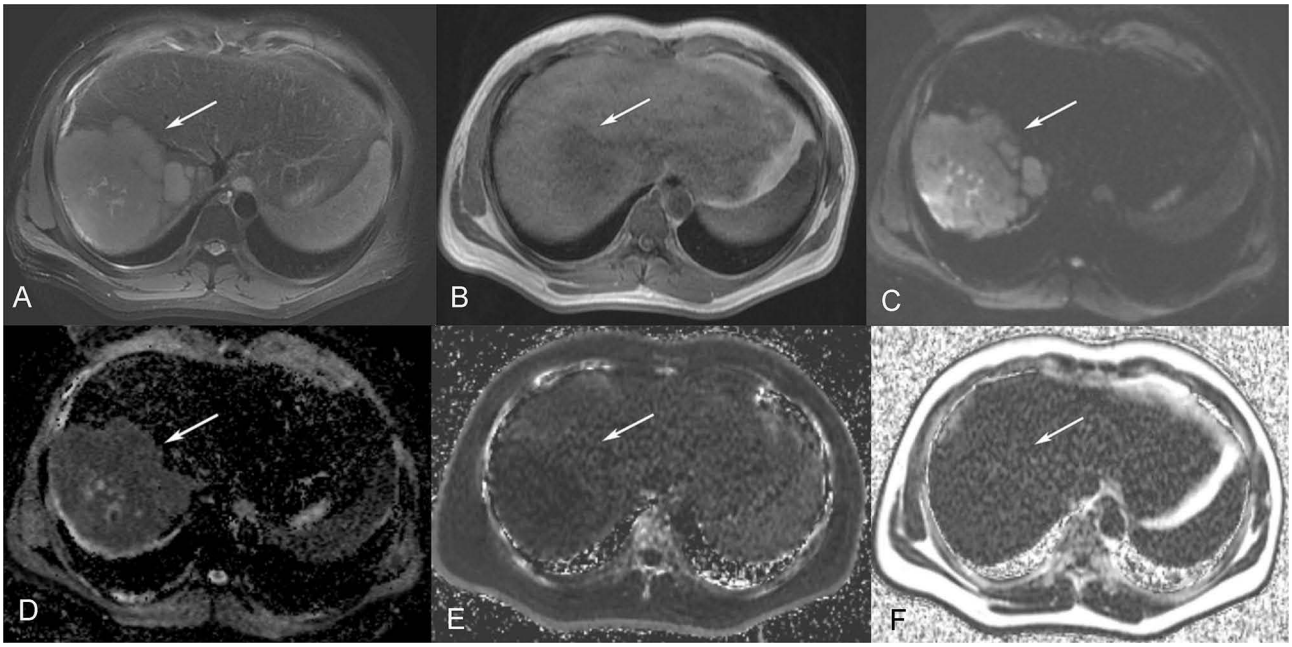

Figure 2 Male patient, 38 years old, pathologically confirmed as P53-mutated HCC (arrows in all panels indicate the target lesion). (**A**) Axial fat-suppressed T2-weighted image (T2WI); (**B**) Axial T1-weighted image (T1WI); (**C**) Diffusion weighted imaging (DWI) map; (**D**) Apparent diffusion coefficient (ADC) map; (**E**) R2* map; (**F**) Fat fraction (FF) map.

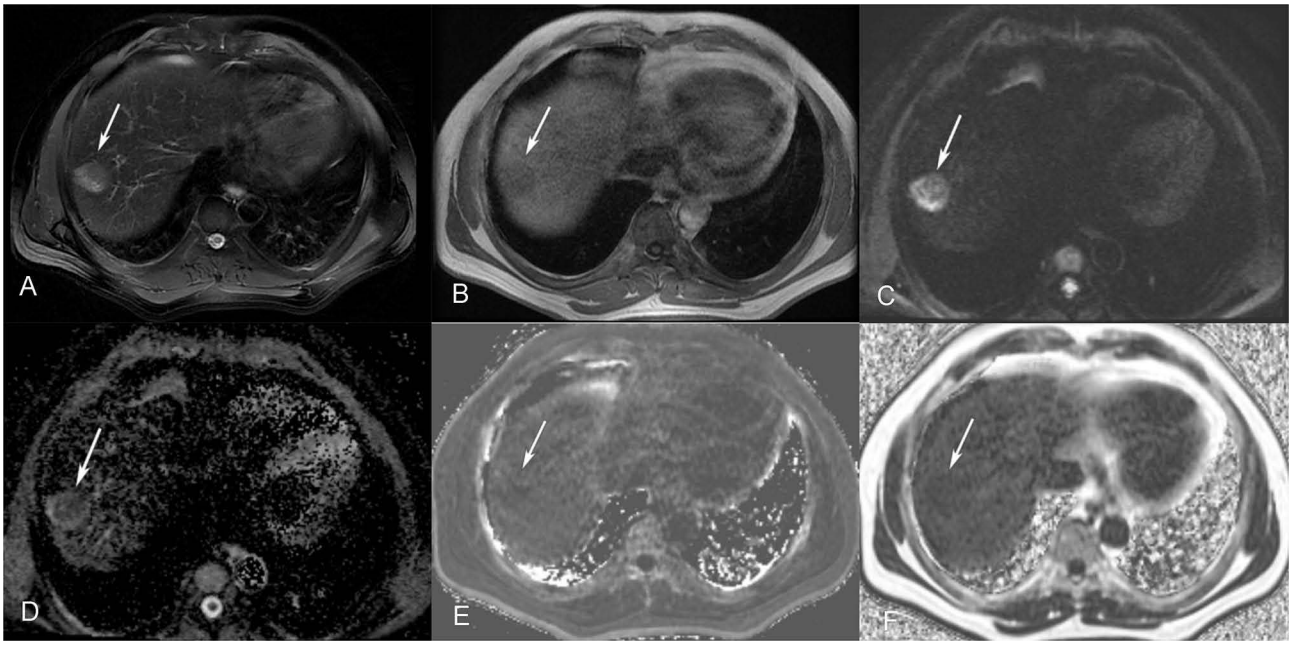

Figure 3 Male patient, 53 years old, pathologically confirmed as non-P53-mutated HCC (arrows in all panels indicate the target lesion). (**A**) Axial fat-suppressed T2-weighted image (T2WI); (**B**) Axial T1-weighted image (T1WI); (**C**) DWI map; (**D**) ADC map; (**E**) R2* map; (**F**) FF map.

Discussion

This study investigates the relationship between P53 mutation status, histological differentiation, and imaging parameters derived from DWI and IDEAL-IQ. IDEAL-IQ quantifies FF and R2* through multi-echo chemical-shift encoding,[18,22] Elevated R2* reflects tumor hypoxia and iron dysregulation via deoxyhemoglobin effects, hallmarking aggressive HCC.[18] In parallel, DWI-derived ADC inversely correlates with cellular density, decreasing in poorly differentiated

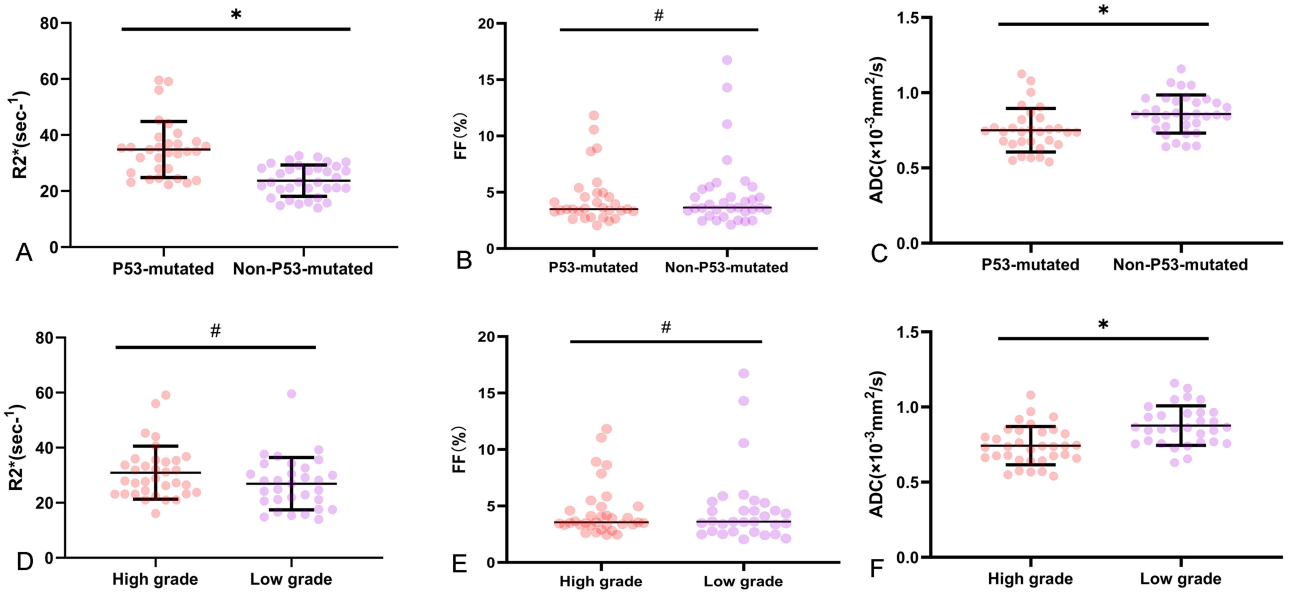

Figure 4 Box plots with scatter points showing multiparametric MRI biomarkers in HCC: (**A**–**C**) P53 mutation contrast: (**A**) R2* (sec^{-1}), (**B**) FF (%), (**C**) ADC ($\times 10^{-3}$ mm^2/s); (**D**–**F**) Histological grade: (**D**) R2* (sec^{-1}), (**E**) FF (%), (**F**) ADC ($\times 10^{-3}$ mm^2/s). *P < 0.05, and #P> 0.05.

tumors.[14] These complementary techniques explain why P53-mutated HCC exhibits higher R2* and lower ADC, capturing hypoxia-driven and microstructural alterations. Our findings demonstrate that R2* and ADC values exhibit strong diagnostic performance in differentiating P53-mutated HCC.

Previous studies investigating the relationship between imaging features and P53 expression are relatively limited. Kitao et al[18] demonstrated that arterial-phase hyperenhancement on dynamic CT and a lower relative enhancement ratio on the hepatobiliary phase of gadoxetic acid-enhanced MRI were independent predictors of P53-mutated HCC. Similarly, Weng et al[20] identified rim enhancement as a potential predictive biomarker for P53-mutated HCC. Our study revealed that P53-mutated HCC had significantly higher R2* values than non-P53-mutated HCC (P < 0.001), while FF values showed no statistical difference in distinguishing P53 expression status (P = 0.646). Interestingly, previous study also found that R2* has excellent potential in predicting Glypican-3 (GPC3) expression in HCC,[18] possibly through tumor microenvironment changes. Hypoxia occurs when tumor metabolic demands exceed oxygen supply, promoting HCC proliferation, angiogenesis, and invasiveness.[23,24] R2* is closely associated with tissue iron content, and its transverse relaxation rate changes correlate linearly with deoxyhemoglobin concentration, reflecting tumor oxygenation.[25] P53 mutations dysregulate the tumor microenvironment via metabolic, vascular, and oxidative stress pathways.[19,23] This elevates intratumoral iron, increasing R2* values. FF primarily reflects tissue fat content. The absence of a significant FF difference implies that P53 mutations exert only limited or indirect effects on fat metabolism. A previous study reported increased fat content in early-stage, well-differentiated steatotic HCC,[26] a trend not observed in our cohort, possibly due to mild steatosis or limited association with P53 mutations. In contrast, our results indicate that P53-mutated HCC has significantly lower ADC values than non-P53-mutated HCC (P = 0.002), suggesting that P53 mutations may be

Table 4 ROC Curve Analysis and DeLong Test Results for R2*, ADC, and the Combined Model

Parameters	AUC (95% CI)	P value	Cut-off value	Youden Index	Sensitivity (%)	Specificity (%)	Compared to Combination (R2*+ADC)	
							Z	P
R2* (sec^{-1})	0.849 (0.739–0.926)	< 0.0001	31.170	0.619	67.74	94.12	0.331	0.741
ADC ($\times 10^{-3}$ mm^2/s)	0.726 (0.602–0.830)	0.0006	0.776	0.507	74.19	76.47	2.069	0.039
Combination (R2* + ADC)	0.856 (0.747–0.931)	< 0.0001	0.660	0.613	61.29	100		

Abbreviations: FF, Fat fraction; ADC, Apparent diffusion coefficient; AUC, Area under the curve; CI, Confidence interval.

https://doi.org/10.2147/JHC.S524533

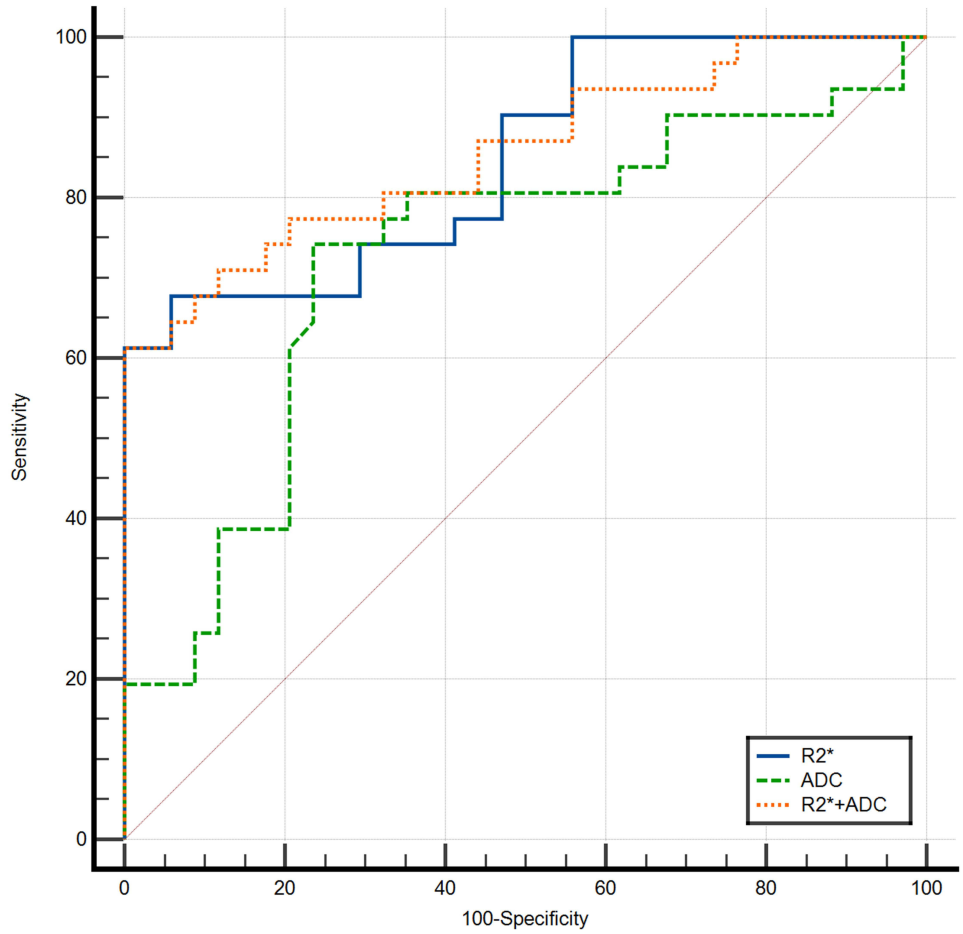

Figure 5 ROC curves of R2*, ADC, and the combined model (R2* + ADC) for predicting P53 mutation in HCC.

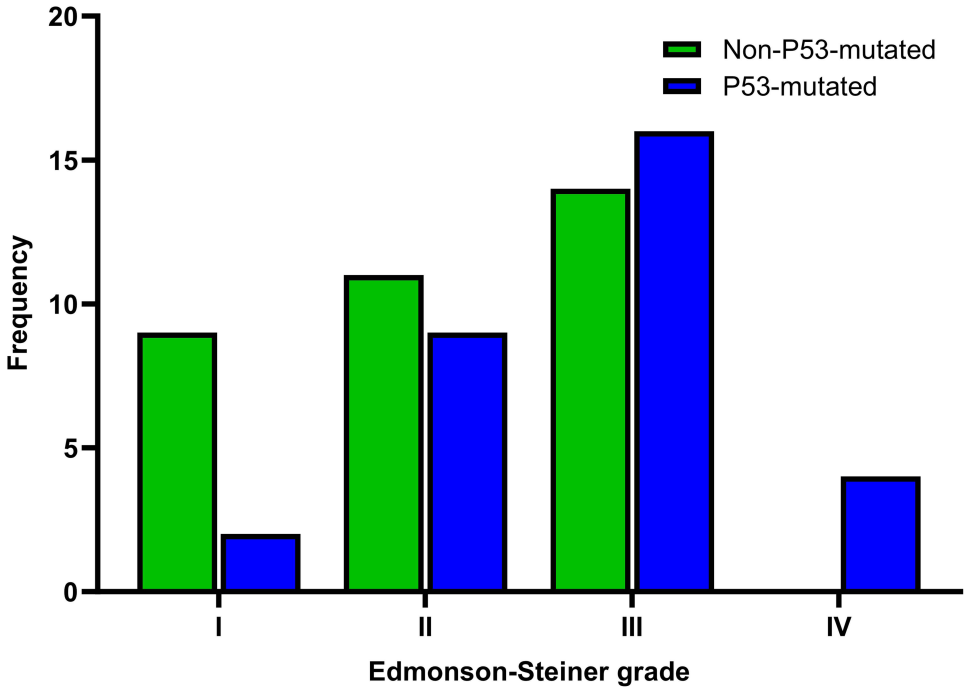

Figure 6 Grouped bar chart showing the distribution of Edmondson-Steiner grades in P53-mutated and non-mutated groups.

associated with higher cell density or more pronounced tumor microenvironment changes in HCC. Previous studies have further suggested that P53-mutated HCC may possess higher malignancy potential and invasiveness, which could correlate with changes in its imaging characteristics.[27–29] Thus, ADC reduction serves as a meaningful imaging marker of these aggressive tumors.

Our study revealed no statistically significant differences in R2* and FF values between high-grade and low-grade HCC ($P > 0.05$), whereas ADC values were significantly lower in the high-grade group ($P < 0.001$), consistent with the findings of Chen et al.[18] Although R2* and FF values reflect magnetic susceptibility and fat content of liver tissue,[17,19] they may be less sensitive to variations in cellular density and microstructure than ADC. Moreover, these parameters may be influenced by physiological factors such as blood flow and liver function,[23,26,30] which do not necessarily differ across histological grades. In contrast, high-grade HCC is often characterized by increased cellular density and complex tissue architecture, restricting water diffusion and resulting in lower ADC values.[31–33] restricting water diffusion and resulting in lower ADC values,[34] supporting ADC as a sensitive biomarker for tumor differentiation.

Our findings indicate that both R2* and ADC are clinically valuable in predicting P53 mutations in HCC. Notably, R2* alone achieved an AUC of 0.849, which was not significantly different from the R2* + ADC model (0.856; $P > 0.05$). This finding aligns with existing literature, which highlights R2* as a sensitive imaging biomarker for reflecting tumor microenvironment, hemodynamic characteristics, and metabolic activity in liver cancer.[18,23] In contrast, ADC, reflecting tissue hydration and cellularity,[35] exhibited weaker discrimination in our cohort. These results suggest that although the combined use of IDEAL-IQ and DWI imaging biomarkers may offer a potential strategy to improve prediction accuracy, R2* alone already demonstrates robust predictive performance. In clinical practice, R2* offers a simple, non-invasive tool for stratifying P53 mutation stratification and personalized management. Future studies should explore the integration of additional imaging biomarkers or molecular features into comprehensive predictive models to further enhance accuracy and broaden clinical applicability.

Additionally, our study found a significant correlation between P53 mutation and Edmondson-Steiner grade ($P = 0.032$). The proportion of P53 mutations was significantly higher in poorly differentiated and undifferentiated tumors, suggesting that P53 mutations may play a role in the loss of differentiation and malignant transformation of tumors. Histological grading is an important indicator for assessing tumor malignancy and prognosis. The relationship between histological grade and P53 mutations may reveal underlying mechanisms of tumor progression and provide new insights into tumor molecular classification and targeted therapy.[36] Previous studies have shown that P53 mutations occur in up to 31% of HCC cases and are often associated with highly proliferative and poorly differentiated HCC.[37] Additionally, other research has demonstrated that P53 expression is correlated with poorly differentiated HCC, indicating a close association with poor prognosis.[38,39] These findings are consistent with our results. Our study further suggests that detecting P53 mutations could serve as a potential marker for evaluating tumor differentiation and aggressiveness. Combined with Edmondson-Steiner grading, this approach may enable a more comprehensive prediction of patients' pathological status and potential disease progression. In summary, our study provides a theoretical basis for developing novel targeted therapies against P53 mutations, such as small-molecule repair agents or inhibitors, particularly for poorly differentiated and undifferentiated tumors, with the aim of improving their unfavorable prognosis.

These imaging biomarkers can be integrated into routine HCC MRI protocols: when IDEAL-IQ and DWI sequences are acquired, radiologists may report $R2^* > 31.170\ sec^{-1}$ or $ADC < 0.776 \times 10^{-3}\ mm^2/s$ to flag likely P53-mutated lesions, prompting multidisciplinary consideration of intensified management.

Despite these promising findings, several limitations should be acknowledged. First, the sample size was relatively small, particularly for HCC patients with P53 mutations, limiting robust subgroup analyses and potentially increasing type II error risk, necessitating larger cohorts to enhance statistical power and generalizability; second, this study focused exclusively on IDEAL-IQ and DWI biomarkers without incorporating complementary molecular markers or imaging modalities such as dynamic contrast-enhanced MRI radiomics, restricting comprehensive mutation prediction, where future integration could significantly improve predictive accuracy; third, despite strict imaging protocols, variability in scanner hardware, field strength, or vendor-specific software could affect data comparability, requiring multi-center validation with standardized protocols to ensure robustness; finally, the retrospective design risks biases including

selection bias, unmeasured confounding, and medical record-dependent information bias, necessitating prospective trials to confirm clinical applicability.

Conclusion

This study underscores the clinical value of IDEAL-IQ and DWI-derived biomarkers, particularly R2* and ADC, in predicting P53 mutations in HCC. R2* demonstrated strong predictive performance, similar to the combined R2* + ADC model, making it a viable standalone biomarker. A significant correlation between P53 mutations and Edmondson-Steiner grade highlights the connection between genetic alterations and tumor differentiation. These findings support the use of advanced imaging for personalized treatment and early intervention, contributing to precision medicine and improved prognostic assessment in liver cancer.

Acknowledgments

The authors would like to thank all participants for their valuable support in this study.

Funding

This study has received funding by the Key Project of Henan Province Medical Science and Technology Project (No. LHGJ20210708), National Natural Science Foundation of China (NSFC, No. 82271978, 92359304, 82330060, 823B2040) and Nanjing Health and Health Commission (YKK21266).

Disclosure

The authors report no conflicts of interest in this work.

References

1. Singal AG, Kanwal F, Llovet JM. Global trends in hepatocellular carcinoma epidemiology: implications for screening, prevention and therapy. *Nat Rev Clin Oncol*. 2023;20(12):864–884. doi:10.1038/s41571-023-00825-3
2. Yue X, Lu Y, Jiang Q, et al. Application of intravoxel incoherent motion in the evaluation of hepatocellular carcinoma after transarterial chemoembolization. *Curr Oncol*. 2022;29(12):9855–9866. doi:10.3390/curroncol29120774
3. Yang C, Zhang S, Cheng Z, et al. Multi-region sequencing with spatial information enables accurate heterogeneity estimation and risk stratification in liver cancer. *Genome Med*. 2022;14(1):142. doi:10.1186/s13073-022-01143-6
4. Kalasekar SM, VanSant-Webb CH, Evason KJ. Intratumor heterogeneity in hepatocellular carcinoma: challenges and opportunities. *Cancers*. 2021;13(21):5524. doi:10.3390/cancers13215524
5. Marei HE, Althani A, Afifi N, et al. p53 signaling in cancer progression and therapy. *Cancer Cell Int*. 2021;21(1):703. doi:10.1186/s12935-021-02396-8
6. Levine AJ. Spontaneous and inherited TP53 genetic alterations. *Oncogene*. 2021;40(41):5975. doi:10.1038/s41388-021-01991-3
7. Khoo KH, Verma CS, Lane DP. Drugging the p53 pathway: understanding the route to clinical efficacy. *Nat Rev Drug Discov*. 2014;13(3):217–236. doi:10.1038/nrd4236
8. Özdemir BH, Özdemir AA. How exercise affects the development and progression of hepatocellular carcinoma by changing the biomolecular status of the tumor microenvironment. *Exp Clin Transplant*. 2022;1–8. doi:10.6002/ect.2021.0456
9. Jeng KS, Sheen IS, Chen BF, Wu JY. Is the p53 gene mutation of prognostic value in hepatocellular carcinoma after resection? *Arch Surg*. 2000;135(11):1329–1333. doi:10.1001/archsurg.135.11.1329
10. Rivlin N, Brosh R, Oren M, Rotter V. Mutations in the p53 tumor suppressor gene: important milestones at the various steps of tumorigenesis. *Genes Cancer*. 2011;2(4):466–474. doi:10.1177/1947601911408889
11. Llovet JM, Kelley RK, Villanueva A, et al. Hepatocellular carcinoma. *Nat Rev Dis Primers*. 2021;7(1):6. doi:10.1038/s41572-020-00240-3
12. Villanueva A, Hoshida Y. Depicting the role of TP53 in hepatocellular carcinoma progression. *J Hepatol*. 2011;55(3):724–725. doi:10.1016/j.jhep.2011.03.018
13. Yuan Z, Li WT, Ye XD, Peng WJ, Xiao XS. Utility of diffusion-weighted imaging to assess hepatocellular carcinoma viability following transarterial chemoembolization. *Oncol Lett*. 2014;8(2):831–836. doi:10.3892/ol.2014.2228
14. Nishie A, Tajima T, Asayama Y, et al. Diagnostic performance of apparent diffusion coefficient for predicting histological grade of hepatocellular carcinoma. *Eur J Radiol*. 2011;80(2):e29–33. doi:10.1016/j.ejrad.2010.06.019
15. Kitagawa T, Kozaka K, Matsubara T, et al. Fat fraction and R2 * values of various liver masses: initial experience with 6-point Dixon method on a 3T MRI system. *Eur J Radiol Open*. 2023;11:100519. doi:10.1016/j.ejro.2023.100519
16. Guo RM, Li QL, Luo ZX, et al. In vivo assessment of neurodegeneration in type C Niemann-pick disease by IDEAL-IQ. *Korean J Radiol*. 2018;19(1):93–100. doi:10.3348/kjr.2018.19.1.93
17. Yang Z, Liu C, Shi Z, Qin J. IDEAL-IQ combined with intravoxel incoherent motion diffusion-weighted imaging for quantitative diagnosis of osteoporosis. *BMC Med Imaging*. 2024;24(1):155. doi:10.1186/s12880-024-01326-0
18. Chen R, Bai Y, Liu T, et al. Evaluation of glypican-3 expression in hepatocellular carcinoma by using IDEAL IQ magnetic resonance imaging. *Acad Radiol*. 2021;28(8):e227–e234. doi:10.1016/j.acra.2020.05.015

19. Peng Y, Zou X, Chen G, et al. Chemical Shift-Encoded Sequence (IDEAL-IQ) and Amide Proton Transfer (APT) MRI for prediction of histopathological factors of rectal cancer. *Bioengineering*. 2023;10(6):720. doi:10.3390/bioengineering10060720
20. Weng J, Xiao Y, Liu J, et al. Exploring the MRI and clinical features of P53-mutated hepatocellular carcinoma. *J Hepatocell Carcinoma*. 2024;11:1653–1674. doi:10.2147/JHC.S462979
21. Rajlawot K, Jiang T, Zhou J, et al. Accuracies of chemical shift in/opposed phase and chemical shift encoded magnetic resonance imaging to detect intratumoral fat in hepatocellular carcinoma. *J Magn Reson Imaging*. 2021;53(6):1791–1802. doi:10.1002/jmri.27539
22. Zheng G, Wei F, Lu P, et al. IDEAL-IQ measurement can distinguish dysplastic nodule from early hepatocellular carcinoma: a case-control study. *Quant Imaging Med Surg*. 2024;14(6):3901–3913. doi:10.21037/qims-23-1593
23. Ren X, Zhao Y, Wang N, et al. Intravoxel incoherent motion and enhanced T2*-weighted angiography for preoperative prediction of microvascular invasion in hepatocellular carcinoma. *Front Oncol*. 2024;14:1389769. doi:10.3389/fonc.2024.1389769
24. Du D, Liu C, Qin M, et al. Metabolic dysregulation and emerging therapeutical targets for hepatocellular carcinoma. *Acta Pharm Sin B*. 2022;12 (2):558–580. doi:10.1016/j.apsb.2021.09.019
25. Zheng H, Zhang H, Zhu Y, Wei X, Liu S, Ren W. Value of blood oxygenation level-dependent magnetic resonance imaging in early evaluation of the response and prognosis of esophageal squamous cell carcinoma treated with definitive chemoradiotherapy: a preliminary study. *BMC Med Imaging*. 2024;24(1):18. doi:10.1186/s12880-024-01193-9
26. Kupczyk PA, Kurt D, Endler C, et al. MRI proton density fat fraction for estimation of tumor grade in steatotic hepatocellular carcinoma. *Eur Radiol*. 2023;33(12):8974–8985. doi:10.1007/s00330-023-09864-x
27. Kitao A, Matsui O, Zhang Y, et al. Dynamic CT and gadoxetic acid-enhanced MRI characteristics of P53-mutated hepatocellular carcinoma. *Radiology*. 2023;306(2):e220531. doi:10.1148/radiol.220531
28. Wang G, Ding F, Chen K, et al. CT-based radiomics nomogram to predict proliferative hepatocellular carcinoma and explore the tumor microenvironment. *J Transl Med*. 2024;22(1):683. doi:10.1186/s12967-024-05393-3
29. Liu X, Guo Y, Zhao L, et al. Can MRI features predict clinically relevant hepatocellular carcinoma genetic subtypes? *Abdom Radiol*. 2023;48 (6):1955–1964. doi:10.1007/s00261-023-03876-3
30. Reeder SB, Cruite I, Hamilton G, Sirlin CB. Quantitative assessment of liver fat with magnetic resonance imaging and spectroscopy. *J Magn Reson Imaging*. 2011;34(4):729–749. doi:10.1002/jmri.22775
31. Nakanishi M, Chuma M, Hige S, et al. Relationship between diffusion-weighted magnetic resonance imaging and histological tumor grading of hepatocellular carcinoma. *Ann Surg Oncol*. 2012;19(4):1302–1309. doi:10.1245/s10434-011-2066-8
32. Lin Y, Luo X, Yu L, et al. Amide proton transfer-weighted MRI for predicting histological grade of hepatocellular carcinoma: comparison with diffusion-weighted imaging. *Quant Imaging Med Surg*. 2019;9(10):1641–1651. doi:10.21037/qims.2019.08.07
33. Wu B, Jia F, Li X, Li L, Wang K, Han D. Comparative study of amide proton transfer imaging and intravoxel incoherent motion imaging for predicting histologic grade of hepatocellular carcinoma. *Front Oncol*. 2020;10:562049. doi:10.3389/fonc.2020.562049
34. Wang W, Guo Y, Zhong J, et al. The clinical significance of microvascular invasion in the surgical planning and postoperative sequential treatment in hepatocellular carcinoma. *Sci Rep*. 2021;11(1):2415. doi:10.1038/s41598-021-82058-x
35. Wang YXJ, Huang H, Zheng CJ, Xiao BH, Chevallier O, Wang W. Diffusion-weighted MRI of the liver: challenges and some solutions for the quantification of apparent diffusion coefficient and intravoxel incoherent motion. *Am J Nucl Med Mol Imaging*. 2021;11(2):107–142.
36. Torbenson M, McCabe CE, O'Brien DR, et al. Morphological heterogeneity in beta-catenin-mutated hepatocellular carcinomas: implications for tumor molecular classification. *Hum Pathol*. 2022;119:15–27. doi:10.1016/j.humpath.2021.09.009
37. Calderaro J, Ziol M, Paradis V, Zucman-Rossi J. Molecular and histological correlations in liver cancer. *J Hepatol*. 2019;71(3):616–630. doi:10.1016/j.jhep.2019.06.001
38. Rahadiani N, Stephanie M, Perkasa AG, Handjari DR, Krisnuhoni E. p53 expression is associated with tumor stage, grade and subtype in patients with hepatocellular carcinoma. *Mol Clin Oncol*. 2023;19(1):54. doi:10.3892/mco.2023.2650
39. You J, Yang H, Lai Y, Simon L, Au J, Burkart AL. AT-rich interactive domain 2, p110α, p53, and β-catenin protein expression in hepatocellular carcinoma and clinicopathologic implications. *Hum Pathol*. 2015;46(4):583–592. doi:10.1016/j.humpath.2015.01.001